Ocean Waves Measurement and Analysis, Fifth International Symposium WAVES 2005, 3rd-7th, July, 2005. Madrid, Spain
Paper number: 221

Numerical Simulation of the December 26, 2004 Indian Ocean Tsunami using a Higher-order Boussinesq Model

Philip Watts[1], Mansour Ioualalen[2], Stéphan Grilli [3], M.ASCE, Fengyan Shi[4] and James T. Kirby[4], M.ASCE

Abstract: Based on differences in seafloor morphology and information about the earthquake, we develop four separate sources for the December 26, 2004 tsunami, along a 1200 km long rupture zone. We trigger these sources in a time sequence spanning 331 s, to perform a numerical simulation of the tsunami, with a higher-order Boussinesq model. We find reasonable agreement of numerical results with a few observed runup values. Our simulation grid is quite fine, although we expect to refine it further in the near future. As more becomes known about the tsunami sources, we will conduct further studies aimed at reproducing tide gage measurements, as well as runup data that is being collected by a variety of international teams.

INTRODUCTION

The December 26, 2004, tsunami is one of the most devastating tsunamis in recorded history. It was generated in the Indian Ocean off of Sumatra by one of the largest earthquakes ever recorded ($M > 9.2$). The number of tsunami fatalities is greater than 200,000 in more than 10 countries across the entire Indian Ocean, although the vast majority of these occurred on the Indonesian island of Sumatra near Banda Aceh. In addition to this disastrous human toll, this tsunami was clearly one of global impact and of global importance, with seismicity and wave action documented around the world for days afterwards. The destruction engendered one of the largest emergency relief efforts ever mounted by world powers and agencies. Scientists had been warning of the growing exposure of coastal residents to tsunami hazards for years, although the location and impact of this event was not anticipated by most. The lack of any effective tsunami education or tsunami warning system in the region exacerbated the number of fatalities, even if many victims on the island of Sumatra, closest to the epicenter, had little chance of escaping the killer waves.

Tsunami observations for this event are voluminous and staggering. Many of these are in the form of still or video camera records of the waves, because the region is a popular

[1]Applied Fluids Engineering, Inc., 5710 E. 7th Street, Long Beach, CA 90803, USA.
[2]Geosciences Azur, (CNRS-IRD), Villefranche-sur-mer, France.
[3]Department of Ocean Engineering, University of Rhode Island (URI), Narragansett, RI 02882, USA; grilli@oce.uri.edu
[4]Center for Applied Coastal Research, University of Delaware, Newark, DE 19761, USA.

tourist destination. These records display a wide variety of wave forms and wave activity that are distinct to each location. In addition, various media recorded numerous eyewitness accounts, including some postings on the world wide web. The quantity of such records, along with their unknown quality, makes the processing and collection of these observations a difficult and lengthy proposition. While we are inclined to use such observations at every opportunity, they are not yet available in a form that we can use here with confidence.

The tsunami community mounted an international response to this event through multiple tsunami survey teams. The survey teams were largely coordinated by the International Tsunami Information Center, a United Nations agency. These teams of scientists documented damage, measured vertical runup and horizontal inundation, and assembled careful reconstructions of wave activity. Each team was restricted to a limited geographical region given the length of damaged coastline and number of countries involved. The runup and inundation data are still becoming available through various publications and web sites, in a piecemeal fashion, region by region. As of now, it appears too early to attempt a complete explanation of tsunami runup and inundation given the scale of the event and the checkerboard pattern of available data.

There have also been a number of instrument records of the December 26, 2004, event in and around the Indian Ocean. These include seismometers, tide gauges, buoys, GPS stations, and at least one satellite overpass (Jason I). These records are quite sparse, both in geographical distribution and in temporal density, and sometimes of poor quality. Regardless, they represent invaluable records of what happened, because of the absolute nature of the data. These data still need careful consideration, because there are often data corrections and interpretations that are needed before any comparison with numerical models can take place. We will not attempt a comprehensive comparison with these records in this work, because this is not the place for such a lengthy analysis. Instead, we propose a first order study of the tsunami, with more detailed analyses and comparisons left for later work. We focus on constructing reasonable tsunami sources, and on explaining the large scale features of tsunami propagation and inundation.

TSUNAMI SOURCES

Large faults must form over time, presumably through small slip events followed in time by larger slip events (Wells and Coppersmith, 1994). Consequently, large single-event displacements tend to occur on structures that have already accumulated large total displacements. Therefore, the structures responsible for the December 26, 2004, event should be evident in the offshore bathymetry, unless they are buried under loose sediment. These structures are generally described as the Australia-Indian (or downgoing) plate subducting beneath the Asian (or overriding) plate, with a largely East-West direction of convergence. The Bay of Bengal consists mostly of the Australia-Indian plate, with a sequence of islands running north-south along the eastern edge of the bay denoting the plate boundaries and the edge of the subduction zone (see Fig. 1a). In the Bay of Bengal, sediment from rivers contribute to a massive sediment fan that covers the entire downgoing plate from north to south, but almost all sediment is diverted West of the overriding plate. The subduction zone is therefore expressed along the entire rupture length, with deformation and erosion of the overriding plate in plain view.

In the case of the December 26, 2004, earthquake, we examine the bathymetry in the Bay

of Bengal in order to describe the morphology of structures visible on the sea floor. The morphology of the sea floor is an expression of the three-dimensional tectonic structures that exist, as well as the tectonic processes that are taking place at depth. In Fig. 1a, we identify four segments with different morphologies along the ruptured subduction zone. These four segments are distinguished by their unique shape and orientation. Let us consider each structure in turn:

1. Segment 1 covers the Southern arc of the ruptured subduction zone, facing in a general South-West direction perpendicular to rupture. The faulting trends North along two relatively sharp bends, one to the north and one to the south of the segment. Here, the overriding plate is at its steepest, and the water depth is largest along the ruptured subduction zone, at around 5100 m in the deepest part of the Java trench.

2. Segment 2 presents a long and relatively straight section of the subduction zone that trends almost North-South along rupture. The most notable feature of this segment is the nearly uniform profile of the overriding plate, with a steep rise from the subduction trench to a shallow ridge, followed by a descent into a deeper basin further East.

3. Segment 3 features a change in orientation and shape, notably a widening of the distance between the subduction zone and the basin to the east. The basin is narrower here, more in the form of a trench. The ridge is shallow enough to form a number of small islands.

4. Segment 4 undergoes a change in orientation, as well as a change in structure, which is more complex and broken than before. A significant number of larger islands are formed on the overriding plate.

Given the different shapes and orientations of the subduction zone described above, we consider each segment as a distinct tsunami source (Fig. 1b). Each tsunami source will have unique and different earthquake parameters that capture the morphology of its own segment. This means that a single rupture event will be represented by a sum of four smaller rupture segments with distinct sea floor morphology.

SEISMIC CHARACTERIZATION

The main shock of the December 26, 2004, earthquake occurred along the subduction zone between the downgoing and overriding plates, at a hypocentral depth of around 25 km from the surface (Tanioka 2005). The main shock epicenter is indicated by a cross on Fig. 1a, with rupture proceeding almost exclusively North from the epicenter (Tanioka 2005). The total rupture length is around 1200 km, requiring a full 400 seconds to propagate end to end at an assumed shear wave speed of around 3000 m/s. Along such a long rupture length, we expect significant slip nonuniformity. This is born out by various seismic inversions, which suggest up to 30 m slip in part of Segments 1 through 3 (Tanioka 2005). Aftershocks occurred along the entire length of the rupture zone.

We point out here that there can be many faults that experienced rupture along the subduction zone, and especially along secondary structures running from the subduction zone up to the surface. These secondary structures are evident in the 3 km high face of stepped (or *en echelon*) thrust faults rising above the subduction trench in Segment 1, and in the rough tapestry (or fabric) of the sea floor on the overriding plate of all segments. It is along these

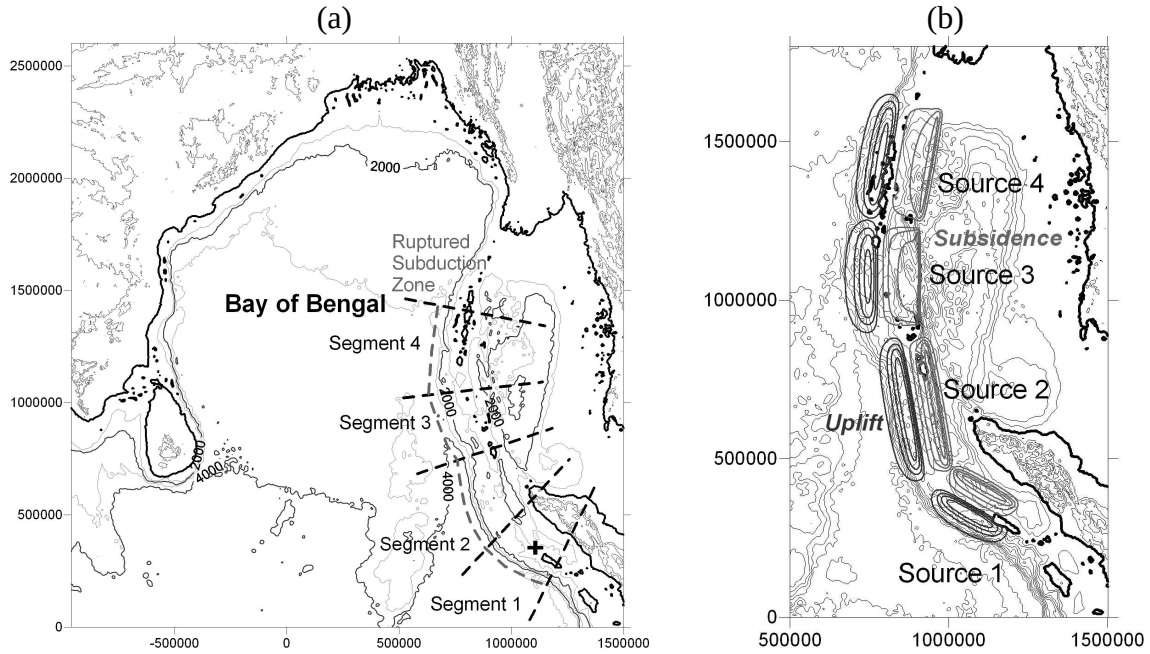

Fig. 1. (a) Simulation grid for the Bay of Bengal. (b) Earthquake tsunami sources along rupture. Axes are in UTM coordinates centered on 0° Lat., 85° Long. E.

secondary faults that coseismic displacement from the main shock is accommodated, with many local variations about the coseismic displacements that we calculate below.

TSUNAMI SIMULATIONS

We simulated the December 26, 2004 event in the Bay of Bengal (Fig. 1a) using ETOPO2 bathymetry and topography data to construct our numerical simulation grid. We converted the decimal degree data into a Universal Transverse Mercator (UTM) projection, with arbitrary origin fixed at 85 degrees east longitude and the equators latitude. We regridded the data using linear interpolation, to produce the uniform grid with 3.4x3.4 km cells, which roughly corresponds to a 2 minute grid spacing. In Fig 1a, the topographic contours are plotted every 500 m, while the bathymetric contours are plotted every 1000 m.

Methodology

The earthquake tsunami sources for vertical coseismic displacement are based in our work on the half-plane solution of an elastic dislocation problem (Okada, 1985). A planar fault of length L and width W is discretized into many small trapezoids and the point source solution of Okada (1985) is used to sum the contributions made by each trapezoid to vertical coseismic displacement, based on the actual depth of the trapezoid. The shear modulus μ can be specified based on the depth d of the earthquake centroid, at latitude-longitude (x_o, y_o), as well as other seismic and geological descriptors. This source was implemented in a software tool, the "Tsunami Open and Progressive Initial Conditions System" (TOPICS, Version 1.2), which provides as outputs, a characteristic tsunami wavelength λ_o that is the smaller of the fault dimensions L or W, and a characteristic initial tsunami amplitude η_o that is the minimum depression found from the coseismic displacement. The seismic moment M_o is proportional to, but slightly less than, $\mu LW\Delta$, because a Gaussian slip distribution is assumed about the centroid, where Δ is the maximum slip. TOPICS allows for the superpo-

sition of multiple fault planes, which can be assembled into complex fault structures or slip distributions.

We simulate tsunami propagation and inundation with FUNWAVE, a public domain higher-order Boussinesq wave model developed over the last ten years at the University of Delaware (Wei and Kirby, 1995; Wei et al., 1995; Chen et al., 2000; Kennedy et al., 2000). FUNWAVE is a fully nonlinear Boussinesq model retaining information to $O\{(kh)^2\}$ in frequency dispersion and to all orders in nonlinearity a/h, where k denotes the wavenumber scale, a denotes a wave amplitude, and h denotes a water depth. Wei et al. (1995) showed that the retention of nonlinear effects beyond the usual order in standard weakly nonlinear Boussinesq models is crucial to the correct modeling of shoaling solitary wave crests, and thus in the present case is important in the modeling of shoreline inundation. The presence of frequency dispersion in the model is important for the case of short wave propagation into relatively deep water, and allows for the mechanism of wave crest splitting during wave propagation over shallow bathymetry. FUNWAVE includes dissipation from breaking waves, and model predictions of shoreline runup have been well tested in the case of wave shoaling and breaking.

We combine TOPICS and FUNWAVE into a single model referred to as Geowave, in which the tsunami sources predicted by TOPICS for a tsunami source are transferred as an initial condition into FUNWAVE. Geowave can simulate multiple tsunami sources with different generation mechanisms, occurring at different times. [The application of this methodology to landslide tsunamis can be found, e.g., in Watts et al. (2003).] The benefits of a Boussinesq wave propagation model over traditional nonlinear shallow water wave models is that the horizontal velocity profile over depth is no longer constrained to have a constant value, and vertical accelerations (i.e., non-hydrostatic pressures) are no longer neglected. During propagation and inundation, non-uniform velocity profiles over depth are most often encountered when water waves propagate in deep water, when water waves runup onto a shoreline of intermediate slope, or when water waves become significantly nonlinear. Dispersive effects are both necessary and manifested during propagation of deep water waves, during propagation of an undular bore in shallow water, and during propagation of edge waves along the coastline (Liu et al., 1998).

Tsunami source parameters

The earthquake parameters for each tsunami source in Fig. 1b are given in Table 1. The total seismic moment release is $M_o = 1.3\,10^{23}$ J, equivalent to MW = 9.4. Most of the tsunami source parameters are similar if not identical along each segment. The location, strike φ, length, and width of each segment follow directly from Fig. 1a. The rake λ and depth d are fixed in the current work, something that we intend to refine further in future work, as more geophysical and geological data become available. The slip Δ captures the seismic inversion results mentioned above. The dip δ varies in such a way as to reproduce the correct distances between sea floor features. The coseismic displacement of each tsunami source is depicted in Fig. 1b , with uplift contours of 1 meter, and with subsidence contours of -2 meters. We note right away that the four tsunami sources do not merge perfectly with one another, although this fact disappears from the wave front in model simulations, within a few minutes of tsunami propagation. We also note that each segment has a different shape of coseismic displacement. These differences arise largely out of the variations in width and dip between each segment, and are intended to mimic sea floor bathymetry.

Table 1. Tsunami source parameters used in TOPICS for Fig. 1.

Parameters	Segment 1	Segment 2	Segment 3	Segment 4
x_o (longitude)	1091550	917000	830000	867300
y_o (latitude)	370600	665000	1075100	1439300
d (km)	25	25	25	25
φ (degrees)	300	350	0	10
λ (degrees)	90	90	90	90
δ (degrees)	11	13	15	11
Δ (m)	30	30	30	25
L (km)	220	410	300	350
W (km)	90	90	150	150
μ (Pa)	$4.0\,10^{10}$	$4.0\,10^{10}$	$4.0\,10^{10}$	$4.0\,10^{10}$
M_o (J)	$1.8\,10^{22}$	$3.4\,10^{22}$	$4.0\,10^{22}$	$4.0\,10^{22}$
λ_o (km)	90	90	150	150
η_o (m)	-9.2	-9.5	-7.6	-7.4

Segment 1 experiences concentrated local uplift along its steep fault scarp. Segment 2 is similarly steep where uplift occurs, and produces a more prominent subsided region where the elongated basin is located. Segment 3 has broader uplift and milder slopes, as well as concentrated subsidence where an abrupt trench exists in the bathymetry. Segment 4 produces uplift in the vicinity of existing islands, whereas the trench is less prominent in both the subsidence and the bathymetry. Not all sea floor features match our calculations perfectly, and there is room to improve all of the tsunami source parameters selected at this stage. For example, the location, strike, depth, and rake of all tsunami sources can be modified in future simulations. However, we have reasonable confidence in our current tsunami sources, because they capture major characteristics of the sea floor morphology.

Tsunami simulations

We perform a numerical simulation of the December 26, 2004, tsunami in the Bay of Bengal by combining the four tsunami sources in Fig. 1 triggered at appropriate times. The first tsunami source, from Segment 1, occurs at the start of the numerical simulation. We calculate the delay between subsequent tsunami sources from the distance between epicentral locations along the rupture path, assuming a shear wave speed of 3000 m/s. Segment 2 ruptures 105 s into the simulation, Segment 3 ruptures 223 s into the simulation, and Segment 4 ruptures 331 s into the simulation. We do not perform simulations where we run each tsunami source separately, because the near field impact and far field propagation are almost uniquely from one or another of the tsunami sources. There should be little confusion as to the origin of the water waves in most impacted regions, because of the long rupture length and directional nature of tsunami propagation.

The maximum tsunami elevations above sea level are depicted in Figs. 2 through 4. The tsunami radiation patterns in Fig. 2 show some dependence on various features of the sea floor. To the West, tsunami propagation depends on the sediment fan that covers most of the Bay of Bengal. To the East, a much more complex pattern emerges due to interference

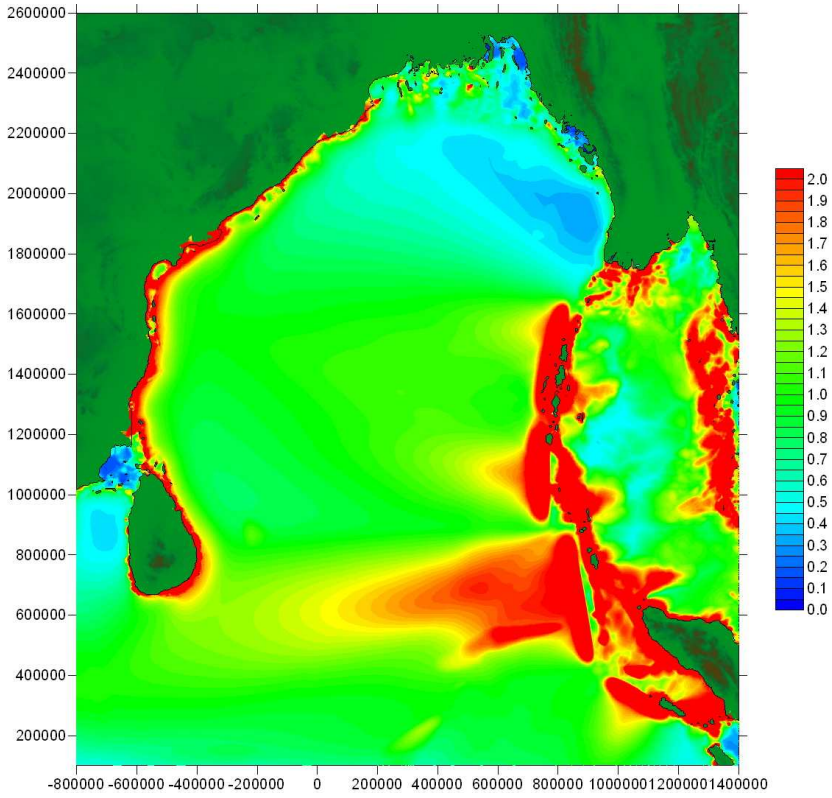

Fig. 2. Maximum simulated tsunami amplitudes in Bay of Bengal.

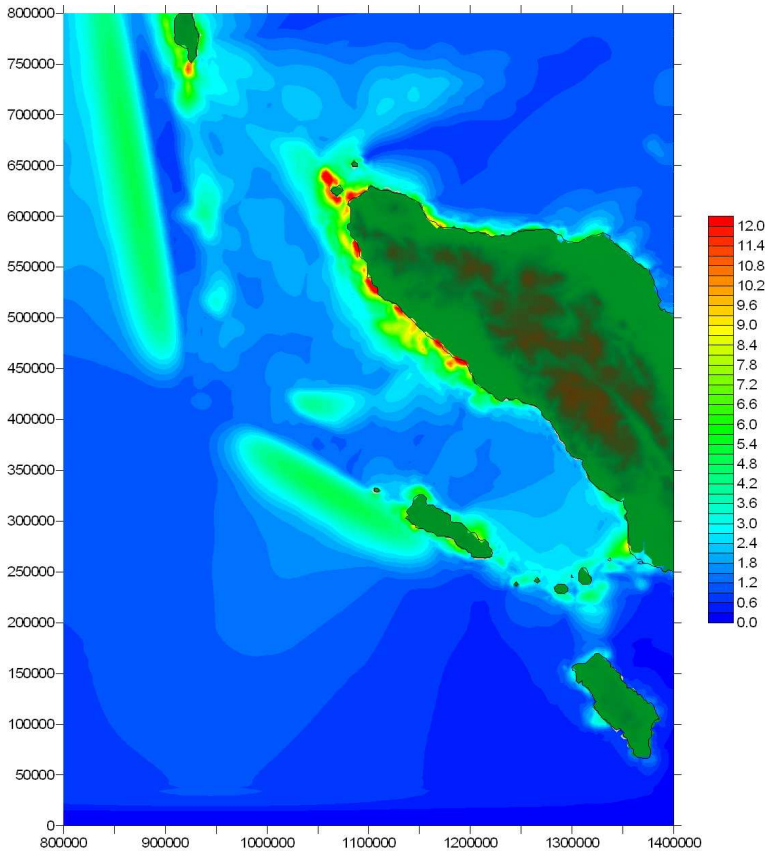

Fig. 3. Details of maximum simulated tsunami amplitudes near Sumatra.

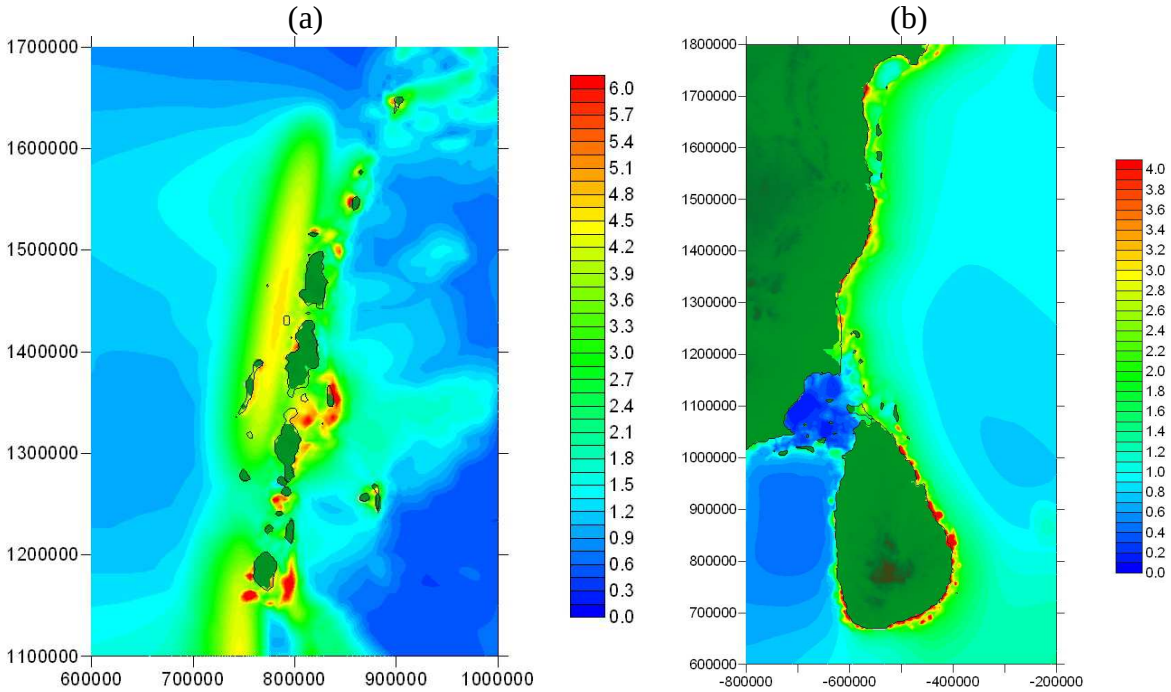

Fig. 4. Details of maximum simulated tsunami amplitudes near : (a) Andaman; (b) Sri Lanka.

Table 2. Simulation results and field survey data (Gusiakov 2005; Harada 2005; Yalciner et al. 2005) at a few key locations.

Locations	Model runup	Model coordinates	Field runup
Aceh, Indonesia	13.8 m	(1082072,618562)	W: 5-35 m; N: 5-10 m
Colombo, Sri Lanka	1.9 m	(-623619,764706)	
Galle, Sri Lanka	2.4 m	(-559060,669542)	
Sri Lanka	5.5 m	(-406160,829281)	2.5-10 m
Chennai, India	3.2 m	(-555663,1519216)	
Nagappaattinam, India	2.4 m	(-627016,1220131)	2-3.5 m
Port Blair, India	5.6 m	(8000555,1294901)	5 m
Rangoon, Burma	1.3 m	(1241768,1927089)	
Phuket, Thailand	4.9 m	(1415055,890457)	S: 3-6 m; W: 5-10 m

and interactions of multiple wave fronts propagating to and among various shorelines. We provide maximum runup values from several locations within the simulation domain in Table 2. The simulated maximum elevations in Figs. 2-4 and the runup values listed in Table 2 compare favorably with observations available from a variety of sources (Gusiakov 2005; Harada 2005; Yalciner et al. 2005). Therefore, we believe that our numerical simulation, although quite preliminary, has captured many of the tsunami features of the actual event.

DISCUSSION OF RESULTS

We point out that the epicenter for the main shock is near a transition point along the subduction zone. This transition point has the appearance of the letter “s”, where there are two sharp bends and a turning point in the curvature. The entire subduction zone has a gentle

curvature similar to those found along almost all major subduction zones. The transition point just off of Sumatra is a remarkable feature, possibly related to the initiation of rupture. North of the transition point, we interpret the decrease in sharp relief and increase in rupture width to an increase in downgoing plate dip, which tends to lower the friction of colliding plates, because the downgoing plate is being pulled towards the earths core by phase change. We hypothesize that the dip is lowest around Segment 1, corresponding to higher friction and locking of the two plates. South of the transition point, we expect the dip angle to increase and the friction to decrease. This hypothesis helps to explain the location of the epicenter and large slip patches off of Sumatra. The rapid changes in subduction zone curvature may be due to rapid changes in flexure of the downgoing plate. The rise of dip angle produces one sharp curvature, whereas the fall of dip angle produces the other sharp curvature.

We posit that it is difficult as of now to attribute any differences between observed and simulated runup values to something specific in our numerical simulation. We have noted before that the tsunami sources can be improved. Moreover, the simulation grid is still not refined enough near certain coastlines to capture the runup process in detail. Likewise, the shallow water bathymetry and coastline details are not available in this work. These are common problems in regional simulations of tsunamis, and therefore suggest a quantum leap in simulation techniques, including unstructured grids. Regardless, the Boussinesq model does a good job of reproducing wave action despite these shortcomings. We are therefore motivated to perform a more detailed study of this event based on our successes to date, using more accurate and detailed field data, as it becomes available.

CONCLUSIONS

We develop four separate sources for the December 26, 2004 tsunami, resulting from a single earthquake occurring along a 1200 km long rupture zone. We relate differences in tsunami source parameters to differences in seafloor morphology. We use these tsunami sources to perform a numerical simulation of the tsunami with a higher-order Boussinesq model, and find reasonable agreement with observed runup values. Our simulation grid is quite fine, although we expect to refine it further in the near future, and exploits the significant capabilities of our Boussinesq wave propagation and inundation model. We are prepared to conduct a more detailed study that takes GPS data into account, and that will be aimed at reproducing measurements available for multiple tide gauges, as well as numerous runup data that is being collected by a variety of international teams of scientists in the Indian Ocean area.

ACKNOWLEDGEMENTS

Partial support from grant CMS-0100223 from the US National Science Foundation is gratefully acknowledged. Partial funding was also provided by Applied Fluids Engineering, Inc. Mention of trade names is for identification purposes only and does not constitute endorsement.

REFERENCES

Chen, Q., Kirby, J. T., Dalrymple, R. A., Kennedy, A. B., and Chawla, A. (2000). "Boussinesq modeling of wave transformation, breaking, and runup. II: 2D." *J. Waterway, Port, Coast, and Ocean Engng.*, 126(1), 48-56.

Gusiakov, V.K. (2005). http://www.pmel.noaa.gov/tsunami/indo20041226/sibolga_nias.htm

Harada, K. (2005). http://www.drs.dpri.kyoto-u.ac.jp/sumatra/thailand/phuket_survey_e.html

Yalciner A.C., Perincek D., Ersoy S., Presateya G., Hidayat R., McAdoo B., (2005). "Report on December 26, 2004, Indian Ocean Tsunami, Field Survey on Jan 21-31 at North of Sumatra", by ITST of UNESCO IOC.

Kennedy, A. B., Chen, Q., Kirby, J. T., and Dalrymple, R. A. (2000).. "Boussinesq modeling of wave transformation, breaking, and runup. I: 1D." *J. Waterway, Port, Coast, and Ocean Engineering*, 126(1), 39-47.

Liu, P. L.-F., Yeh, H., Lin, P., Chang, K.-T., and Cho, Y.-S. (1998). "Generation and evolution of edge wave packets." *Phys. Fluids*, 10(7), 1635-1657.

Okada, Y. (1985). "Surface deformation due to shear and tensile faults in a half-space." *Bull. Seis. Soc. Am.*, 75(4), 1135-1154.

Tanioka, Y. (2005). Personal Communication, April 2, 2005.

Watts, P., Grilli, S. T., Kirby, J. T., Fryer, G. J., and Tappin, D. R. (2003). "Landslide tsunami case studies using a Boussinesq model and a fully nonlinear tsunami generation model." *Nat. Hazards and Earth Sci. Systems*, 3(5), 391-402.

Wei, G., and Kirby, J. T. (1995). "Time-dependent numerical code for extended Boussinesq equations." *J. Waterway, Port, Coast, and Ocean Engng.*, 121(5), 251-261.

Wei, G., Kirby, J. T., Grilli, S. T., and Subramanya, R. (1995). "A fully nonlinear Boussinesq model for free surface waves. Part 1: Highly nonlinear unsteady waves" *J. Fluid Mech.*, 294, 71-92.

Wells, D.L., and Coppersmith, K.J. (1994). "New empirical relationships among magnitude, rupture length, rupture width, rupture area, and surface displacement." *Bull. Seismological Soc. of America*, 84, 974-1002.